

Controllable design of nanoworm-like nickel sulfides for efficient electrochemical water splitting in alkaline media

Author

Chen, Z, Ibrahim, I, Hao, D, Liu, X, Wu, L, Wei, W, Su, D, Ni, B-J

Published

2020

Journal Title

Materials Today Energy

Version

Accepted Manuscript (AM)

DOI

[10.1016/j.mtener.2020.100573](https://doi.org/10.1016/j.mtener.2020.100573)

Rights statement

© 2020 Elsevier. Licensed under the Creative Commons Attribution-NonCommercial-NoDerivatives 4.0 International Licence (<http://creativecommons.org/licenses/by-nc-nd/4.0/>) which permits unrestricted, non-commercial use, distribution and reproduction in any medium, providing that the work is properly cited.

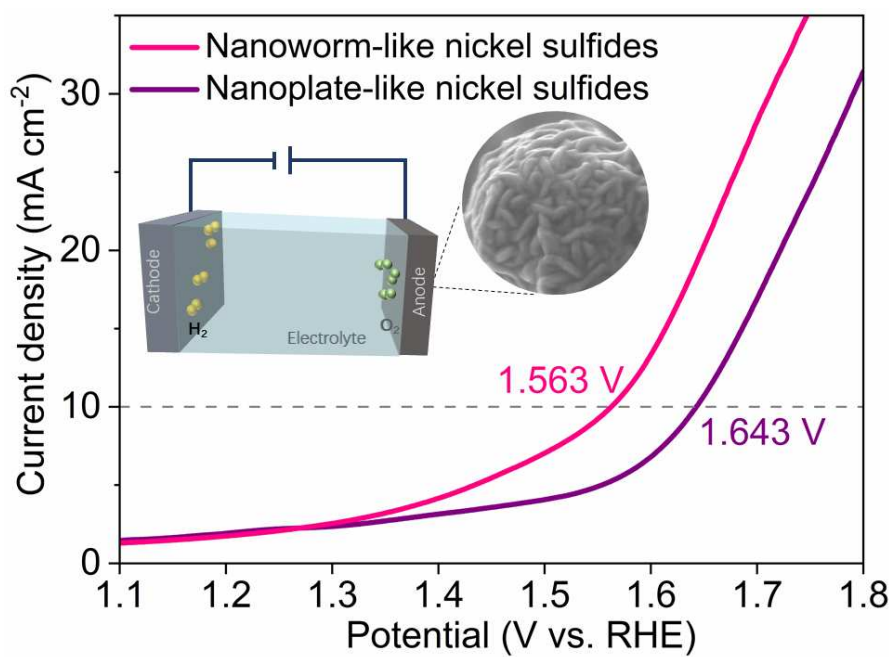
Downloaded from

<http://hdl.handle.net/10072/412047>

Griffith Research Online

<https://research-repository.griffith.edu.au>

Graphical Abstract



The nanoworm-like nickel sulfides developed by a one-step solvothermal strategy exhibit great performance for overall electrochemical water splitting, and a low voltage of 1.563 V is required to attain a current density of 10 mA cm⁻² in a two-electrode electrolyzer.

1 **Controllable design of nanoworm-like nickel sulfides for efficient**
2 **electrochemical water splitting in alkaline media**

3 Zhijie Chen,^a Idris Ibrahim,^a Derek Hao,^a Xiaoqing Liu,^a Lan Wu,^a Wei Wei,^a Dawei
4 Su,^{b,*} Bing-Jie Ni ^{a,*}

5

6 ^a *Centre for Technology in Water and Wastewater, School of Civil and Environmental*
7 *Engineering, University of Technology Sydney, NSW 2007, Australia*

8 ^b *Center for Clean Energy Technology, School of Mathematical and Physical Science,*
9 *Faculty of Science, University of Technology Sydney, NSW 2007, Australia*

10

11

12

13

14

15

16

17

18

19

20

21

22

23

24

25 *Corresponding Author:

26 Dawei Su E-mail: Dawei.Su@uts.edu.au

27 Bing-Jie Ni E-mail: bingjieni@gmail.com

28

29

30 **Abstract**

31 Developing cost-effective electrocatalysts for electrochemical water splitting (EWS) is appealing
32 and challenging for sustainable water electrolysis. Currently, nickel sulfides are considered as
33 promising candidates for EWS due to their low cost and high catalytic activity. However, the
34 facile design of nickel sulfides with high catalytic performance is still highly demanded. In this
35 study, we have developed a one-step solvothermal strategy to construct nickel sulfides as efficient
36 water splitting catalysts. By taking advantage of the small size, abundant active sites, large
37 electrochemical surface area, and good conductivity, the nanoworm-like nickel sulfides
38 (NiS-NW/NF) exhibit better OER performance (a low overpotential of 279 mV to achieve 100 mA
39 cm^{-2} , Tafel slope of 38.44 mV dce^{-1}) than the nanoplate-like analogues, as well as most of reported
40 nickel sulfide-based electrocatalysts. Additionally, the NiS-NW/NF directly used as bifunctional
41 electrodes for overall water splitting requires a low voltage of 1.563 V to attain a current density
42 of 10 mA cm^{-2} with good long-term durability. This work provides a facile strategy for the design
43 of efficient nickel sulfide-based electrocatalysts for energy conversion applications.

44

45 **Keywords:** Nickel sulfides; Morphology; Solvothermal synthesis; Oxygen evolution reaction;

46 Overall water splitting

47

48 **1. Introduction**

49 Developing renewable energy technologies is an urgent issue to mitigate the impending energy
50 crisis and the alarming environmental degradation. Electrochemical water splitting (EWS) is an
51 efficient and clean way to produce hydrogen which is considered as a green energy carrier [1-3].
52 The EWS consists of two half reactions, the hydrogen evolution reaction (HER) at the cathode and
53 the oxygen evolution reaction (OER) at the anode. Importantly, the efficiency of the EWS is
54 highly dependent on the electrode materials, namely the catalysts. Noble metal (e.g., Pt, Ir, Pd, and
55 Ru)-based catalysts have exhibited great performance for EWS, however the low reserve and high
56 price of these materials significantly limit their commercial applications [4, 5]. As a result, it is
57 imperative to develop low-cost and efficient electrocatalysts for EWS. To our delight, numerous
58 earth-abundant materials have shown good catalytic performance for EWS [6], including
59 transition metal-based materials [7-12] and metal-free materials [13-17]. Among these low-cost
60 candidates, transition metal sulfides (TMSs) have attracted enormous attention as OER and HER
61 catalysts due to the high intrinsic catalytic activity, good electrical conductivity, and structural
62 stability.

63 Nanoscale TMSs have been widely studied for EWS, but their catalytic performance is still
64 inferior to that of precious metal-based materials. To further improve the catalytic properties of
65 TMSs, various efficient strategies have been employed, including chemical component regulation
66 [1, 18], morphology control [19, 20], defect engineering [21, 22], and hybridization [23, 24], etc.
67 Recent studies show that the morphology of nanocatalysts has a prominent effect on the catalytic
68 performance of TMSs [25]. For example, Wu et al. [26] compared the catalytic performance of

69 three zinc cobalt mixed sulfide nanostructures with different morphologies, including nanosheets,
70 nanoplates, and nanoneedles. The one-dimensional Zn-Co-S nanoneedles exhibited higher
71 catalytic activities toward both HER and OER than the analogues. This is because the integrated
72 Zn-Co-S nanoneedle/CFP nanostructure can provide enhanced electrochemical active area,
73 facilitate ion transfer, and gas evolution. Similarly, You and co-workers investigated the
74 correlation between morphology and HER activity of a series of CoS with different morphologies
75 (hollow nanoprism, broken nanoprism, and nanoparticle) [27]. The CoS nanoparticle shows the
76 largest specific surface area and electrochemically active surface area (ECSA), and these features
77 result in the improved accessibility of electroactive sites, enhanced mass/charge transport and
78 accelerated release of gas bubbles, rendering its highest HER performance and good durability. As
79 a result, it is of great significance to tune the morphology of catalysts, and thus improve the
80 surface active sites and the structural stability [28]. Although TMSs with different morphologies
81 for EWS have been documented, the morphology-control synthesis of efficient NiS catalysts with
82 facile methods is still challenging. Additionally, the relationship between the
83 morphology-controlled catalysts and their catalytic properties needs further explorations.

84 Herein, we have developed a one-step solvothermal strategy to construct nickel sulfides as
85 efficient water splitting catalysts. The morphology-dependent electrochemical performance is
86 uncovered, and the nanoworm-like nickel sulfides (NiS-NW/NF) outperform the nanoplate-like
87 counterpart. Benefiting from the small size, abundant active sites, large electrochemical surface
88 area, and good conductivity, the NiS-NW/NF exhibits great OER performance (e.g., $\eta_{100} = 279$
89 mV, Tafel slope = 38.44 mV dce⁻¹) and good HER activity. When fabricated in a two-electrode cell,

90 only a voltage as low as 1.563 V was required to achieve a current density of 10 mA cm⁻².

91 **2. Experimental section**

92 **2.1. Material synthesis**

93 The NiS nanoworms (NW) were prepared using a solvothermal method. Briefly, Ni foam (NF)
94 with a thickness of 1 mm was ultrasonically treated with 1M HCl, followed by acetone (≥99.5%,
95 Sigma-Aldrich) and distilled water in order to remove the oxide layer. The growth solution was
96 prepared by dissolving 2 mmol of thiourea (TU, ≥99.0%, Sigma-Aldrich) as sulfur source into 27
97 ml of isopropanol alcohol (IA, ≥99.5%, Sigma-Aldrich) under vigorous stirring at room
98 temperature for 1 hour. After TU completed dissolved, 3 ml of glycerol (≥99.5%, Sigma-Aldrich)
99 was added to the solution and continues stirring for another 30 min. Then, the mixed solution was
100 transferred into a 50 ml autoclave followed by immersing NF (2 × 2 cm²) and placed at a
101 conventional oven at 180 °C for 3 hours. After the reaction completed it allowed to be cooled
102 naturally. Finally, the as-obtained materials were washed with water and ethanol several times and
103 dried at the vacuum oven for 4 h at 60 °C. Similarly, the NiS nanoplates (NP) were synthesized
104 when 30 ml of IA was used, without the addition of glycerol. A series of NiS samples were
105 prepared via changing the dosages of IA and glycerol, and the total amount of IA and glycerol was
106 controlled at 30 ml.

107 **2.2. Structural characterization**

108 The structural morphology of the samples was analyzed using scanning electron microscopy
109 (SEM, Zeiss Sigma 55VP). The crystal structure of the samples was determined by X-ray

110 diffraction (XRD) measurements on a Rigaku Smart Lab X-ray diffractometer operated at 40 kV
111 using Cu K α radiation. Transmission electron microscope (TEM) images were performed with a
112 FEI Tecnai G2 F20 S-TWIN microscope with an acceleration voltage of 200 kV. The element
113 composition of the material was analyzed by the X-ray photoelectron spectroscopy (XPS, Thermo
114 K-Alpha⁺, Thermo Fisher Scientific, USA) with the Al (K α) radiation.

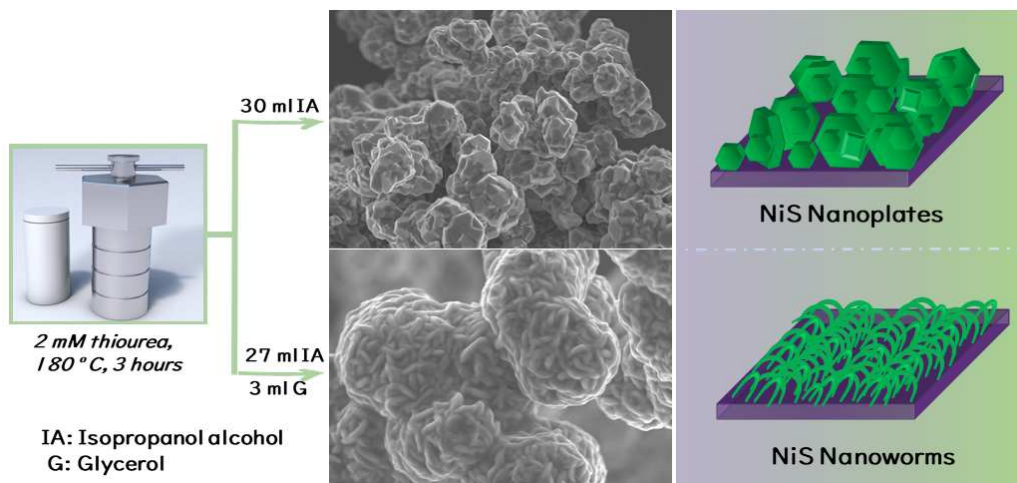
115 **2.3. Electrochemical measurements**

116 Electrochemical measurements were carried out with a CHI 760E electrochemical workstation.
117 OER and HER activities were recorded in a three-electrode system with graphite rod as the
118 counter electrode and Hg/HgO as the reference electrode in O₂-saturated and N₂-saturated 1.0 M
119 KOH electrolytes, respectively. The as-prepared NF-supported samples were directly used as the
120 working electrode. To prepare the IrO₂ electrode, 5 mg of IrO₂ powder (99.9%, Sigma-Aldrich)
121 were dispersed in 1 mL of mixed solution (500 μ L of water, 450 μ L of ethanol, and 50 μ L of 5 wt%
122 Nafion solution). The 20 wt % Pt/C electrode was prepared with a similar process. After
123 sonication for 30 min, a homogeneous ink was obtained. 100 μ L of the ink was deposited onto a
124 piece of acid treated NF. Linear sweep voltammetry (LSV) was performed at scan rate of 5 mV s⁻¹
125 for both HER and OER. The polarization curves were calibrated with 90% iR compensation to
126 eliminate the solution resistance. All potentials measured were converted to a reversible hydrogen
127 electrode (RHE) using the following equation: $E_{\text{vs RHE}} = E_{\text{vs Hg/HgO}} + 0.098 \text{ V} + 0.059 \text{ pH}$.
128 Electrochemical impedance spectroscopy (EIS) was recorded at the open circuit potential over a
129 frequency range of 10⁻¹ to 10⁵ Hz with an AC signal amplitude of 5 mV. The double-layer
130 capacitances (C_{dl}) were calculated through cyclic voltammogram (CV) at different scan rates (i.e.,

131 40, 60, 80, 100, and 120 mV s^{-1}) in 1.0 M KOH. The Amperometric i-t curves were recorded to
132 test the long-term stability of catalysts for both OER and HER, and for the overall water splitting.

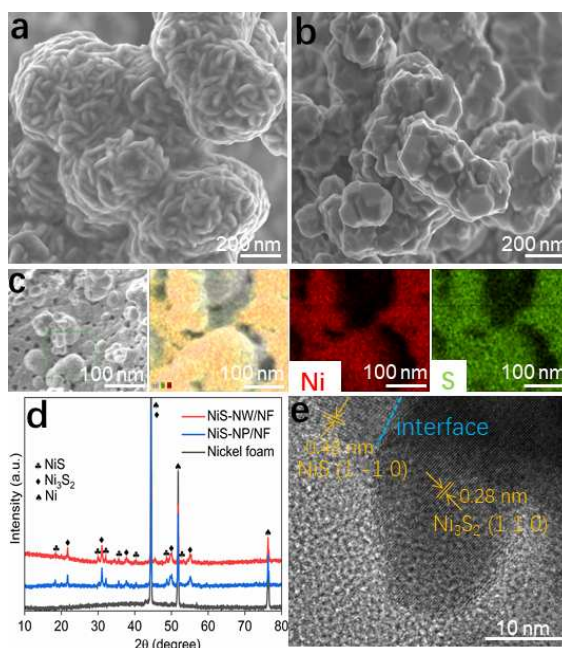
133 3. Results and discussion

134 3.1. Material characterizations



136 **Fig. 1** Schematic of the formation of NiS-NW/NF and NiS-NP/NF.

137 **Fig. 1** illustrates the synthesis procedure of the nickel sulfide samples, which only comprises a
138 solvothermal sulfidization of direct growth of nickel sulfides on nickel foam. The appropriate
139 addition of glycerol and IA as surfactants is the key for tuning the morphology of nickel sulfides.
140 The nanoworm-like nickel sulfide sample (NiS-NW/NF) is obtained when a small amount (3 ml)
141 of glycerol and 27 ml of IA are added as the solvent, while the nanoplate-like nickel sulfide
142 sample (NiS-NP/NF) is formed with adding 30 ml of IA only. Compared with the NiS-NP/NF, the
143 NiS-NW/NF possesses a smaller average size (~ 100 nm vs ~ 200 nm) and higher surface area (**Fig.**
144 **2a-b**). These features suggest that the NiS NWs may be more favorable for electrochemical
145 reactions than the counterpart. In addition, the energy-dispersive spectroscopy (EDS) elemental
146 mapping images of the NiS NWs (**Fig. 2c**) show the uniformly distribution of Ni and S.



147

148 **Fig. 2** (a) SEM image of NiS-NW/NF, (b) SEM image of NiS-NP/NF, (c) SEM-EDS mapping of

149 NiS-NW/NF, (d) XRD patterns of NiS-NW/NF, NiS-NP/NF and bare Nickel foam, (e) HRTEM image

150 of NiS-NW/NF.

151 The crystal structures of the as-prepared nickel sulfides were investigated with XRD. As depicted

152 in **Fig. 2d**, most of the strong peaks in the XRD patterns of NiS-NW/NF and NiS-NP/NF are

153 matched to Ni₃S₂ (JCPDS No. 71-1682) and NiS (JCPDS No. 86-2280), indicating that the two

154 nickel sulfide samples are mainly composed of Ni₃S₂ and NiS. The diffraction peaks at 21.7°,

155 31.0°, 37.7°, 38.2°, 44.3°, 49.6°, 50.0°, and 55.2° can be assigned to (1 0 1), (1 1 0), (0 0 3), (0 2 1),

156 (2 0 2), (1 1 3), (2 1 1), and (1 2 2) reflection planes of Ni₃S₂, respectively; whereas those at 18.3°,

157 30.2°, 32.1°, 35.7°, 40.4°, 48.8°, 50.1°, 52.6°, and 57.3° can be indexed to (1 -1 0), (1 0 1), (3 0 0),

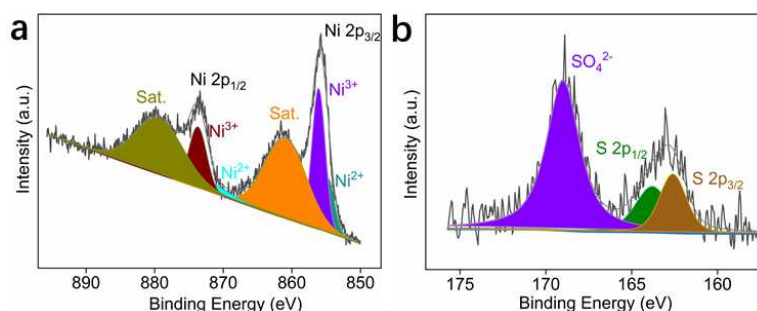
158 (0 2 1), (2 1 1), (1 3 1), (4 1 0), (4 0 1), and (3 3 0) reflection planes of NiS, respectively. Apart

159 from Ni₃S₂ and NiS, the strong peaks of metallic Ni are still observed on the patterns of nickel

160 sulfide samples, suggesting that the nickel foam is partially sulfurized. Further insights into the

161 nanostructure of NiS NWs are provided by the TEM analysis. **Fig. 2e** presents a typical high
162 magnification TEM image of NiS NWs, the crystal lattices of NiS NWs can be indexed to Ni₃S₂
163 and NiS with a clear interface. The lattice distances of 0.28 and 0.48 nm correspond to the (1 1 0)
164 and (1 -1 0) crystal planes of Ni₃S₂ and NiS, respectively. The results from the TEM image are
165 line with the XRD analysis.

166 X-ray photoelectron spectroscopic (XPS) analysis was employed to ascertain the elemental
167 composition and the electronic structure of the NiS-NW/NF sample. The survey spectrum
168 suggests the presence of Ni and S elements in the sample (**Fig. S1**). As depicted in **Fig. 3a**, the
169 appreciable peaks at 854.7 and 872.1 eV are attributed to the Ni²⁺ state, and the distinct peaks at
170 856.1 and 873.7 eV are correspond to the Ni³⁺ state. These results suggest the co-existence of NiS
171 and Ni₃S₂ in NiS-NW/NF [29]. Meanwhile, the high-resolution spectrum of S 2p in **Fig. 3b**
172 displays three fitting peaks at 169.1 eV, 163.8 eV and 162.6 eV, which can be assigned to SO₄²⁻, S
173 2p_{1/2} and S 2p_{3/2} in NiS-NW/NF, respectively, and the presence of SO₄²⁻ is mainly due to surface
174 oxidation.

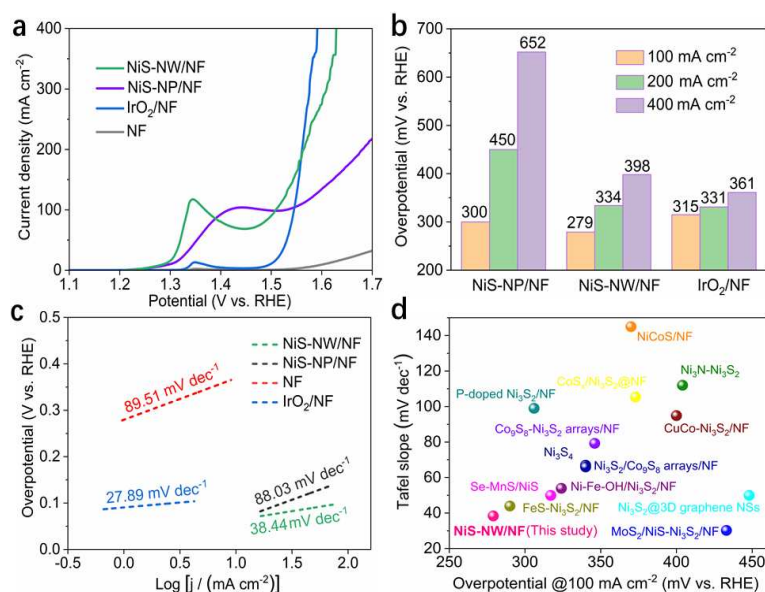


175
176 **Figure 3.** XPS spectra of NiS-NW/NF. (a) the Ni 2p spectrum and (b) the S 2p spectrum.

177 3.2. Electrocatalytic performance

178 The oxygen evolution activity of the as-prepared nickel sulfide samples was examined in the

179 oxygen-saturated 1.0 M KOH solution. For comparison, the OER performances of acid treated
180 bare NF and IrO₂/NF were also tested under the same experimental conditions. As shown in **Fig.**
181 **4a**, NiS-NW/NF requires a substantial lower overpotential of 279 mV to obtain 100 mA cm⁻²
182 compared to NiS-NP/NF (300 mV), and IrO₂/NF (315 mV). The peaks ranging from 1.3 to 1.4 V
183 vs. RHE for the LSV curves of are ascribed to the oxidation of Ni²⁺ to Ni³⁺. Furthermore, at the
184 anodic current densities of 200 mA cm⁻² and 400 mA cm⁻², the applied overpotential of
185 NiS-NW/NF are 334 mV and 398 mV respectively, significantly lower than those of NiS-NP/NF
186 (450 mV and 652 mV) (**Fig. 4b**). **Fig. 4c** shows that NiS-NW/NF delivers a lower Tafel slope
187 (38.44 mV dce⁻¹) than NiS-NP/NF (88.03 mV dce⁻¹) and NF (89.51 mV dce⁻¹), suggesting the
188 OER kinetics of NiS-NW/NF is superior to the that of NiS-NP/NF and NF. These results of
189 overpotentials and Tafel slopes reveal that NiS-NW/NF indeed exhibits efficient OER
190 performances ($\eta_{100} = 279$ mV, Tafel slope = 38.44 mV dce⁻¹), which are much better than
191 NiS-NP/NF ($\eta_{100} = 300$ mV, Tafel slope = 88.03 mV dce⁻¹). In addition, the OER activities (η_{100} ,
192 Tafel slope) of NiS-NW/NF outperform most of recently documented nickel sulfide-based OER
193 catalysts (**Fig. 4d**) [29-41], such as NiCoS/NF (370 mV, 145 mV dce⁻¹) [36], Ni₃N-Ni₃S₂ (404 mV,
194 112 mV dce⁻¹) [37], CoS_x/Ni₃S₂@NF (373 mV, 105 mV dce⁻¹) [38], P-doped Ni₃S₂/NF (306 mV,
195 99 mV dce⁻¹) [39], Ni₃S₄ (340 mV, 67 mV dce⁻¹) [41].



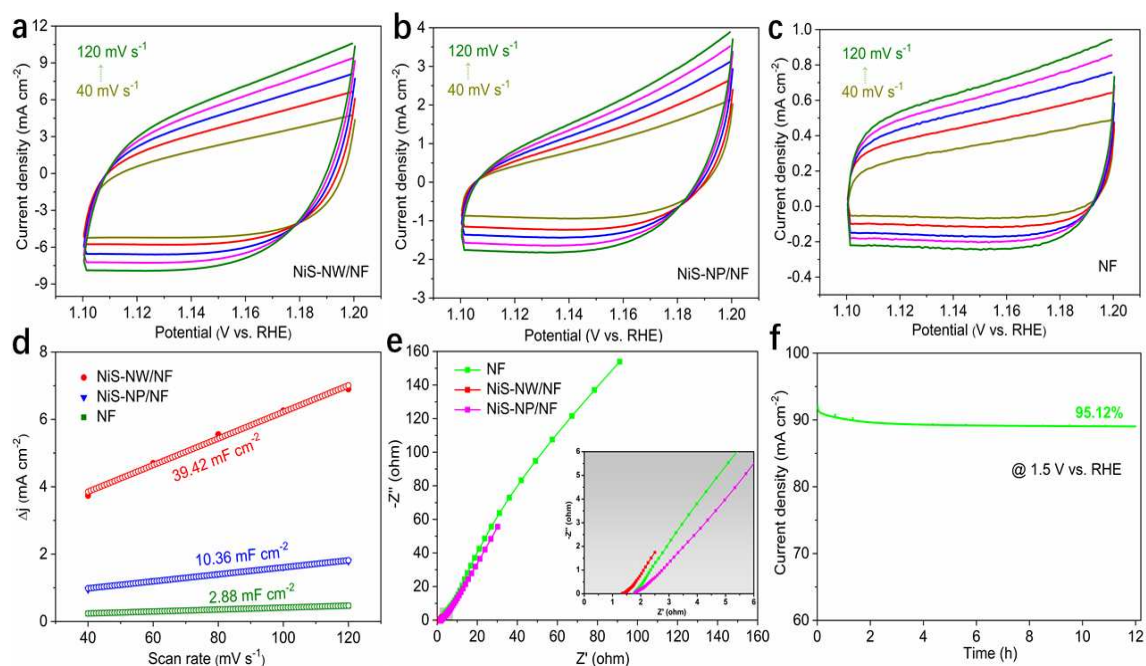
196

197 **Fig. 4** (a) LSV curves of the OER performance of Ni foam, NiS-NW/NF, NiS-NP/NF, and IrO₂/NF in
 198 1.0 M KOH at a scan rate of 5 mV s⁻¹. (b) Comparison of overpotentials at 100, 200, and 400 mA cm⁻²
 199 of NiS-NW/NF, NiS-NP/NF, and IrO₂/NF. (c) Tafel plots of Ni foam, NiS-NW/NF, NiS-NP/NF, and
 200 IrO₂/NF. (d) Comparison of overpotential and Tafel slope of OER between the NiS-NW/NF and
 201 reported nickel sulfide-based catalysts.

202 To probe the charge-transfer kinetics and the ECSA of catalysts, C_{dl} and EIS were measured. C_{dl} is
 203 a convincing parameter for the estimation of accessible active sites of electrocatalysts, as the C_{dl} is
 204 positively proportional to ECSA (ECSA = C_{dl}/C_s, where C_s is the specific capacitance). The C_{dl}
 205 was measured via CV scans in the non-faradic potential region (1.1 - 1.2 V vs. RHE) at various
 206 scan rates (40, 60, 80, 100, 120 mV/s) (**Fig. 5a-c**). The capacitive current density differences (Δ
 207 $j = (j_a - j_c)/2$) at 1.15 V vs. RHE as a function of scan rate displays the C_{dl} values of catalysts (**Fig.**
 208 **5d**). The calculated C_{dl} values of NiS-NW/NF, NiS-NP/NF and NF are 39.42, 10.36, and 2.88 mF
 209 cm⁻², respectively. The high C_{dl} value means NiS-NW/NF possesses a much higher ECSA in

210 comparison to that of NiS-NP/NF and NF, suggesting that NiS-NW/NF exposes more
211 electroactive sites for the electrocatalytic water oxidation reaction. To further investigate the OER
212 kinetics, EIS was also measured. **Fig. 5e** presents the Nyquist plots of NiS-NW/NF, NiS-NP/NF
213 and NF. The Nyquist plot of NiS-NW/NF shows a smaller semicircle than that of NiS-NP/NF and
214 NF in the high frequency region. The fitting results suggest that NiS-NW/NF exhibits a smaller
215 charge transfer resistance (R_{ct}) (4.84 Ω) than that of NiS-NP/NF (21.11 Ω) and NF (67.11 Ω),
216 revealing faster charge transfer and the smaller charge transfer resistance of the NiS-NW/NF
217 during the OER process.

218 In this study, the chronoamperometry (CA) measurement was conducted at a constant potential of
219 1.5 V vs. RHE to evaluate the durability of NiS-NW/NF toward OER. As depicted in **Fig. 5f**, the
220 current density remains stable after 12 h running, and only about 5% current density loss happened
221 on the NiS-NW/NF electrode. This result indicates that the NiS-NW/NF exhibits good stability
222 under alkaline conditions. In addition, the XPS test was performed to examine the chemical state
223 of the pre-catalytic and post-OER NiS-NW/NF. There is no obvious change observed for signals
224 for the Ni species (**Fig. S2**) for the catalyst after the OER electrocatalysis. However, the S 2p
225 spectra show that the intensity of S peaks decreases significantly after the long-term OER test (**Fig.**
226 **S3**), indicating the surface oxidation of NiS-NW/NF.



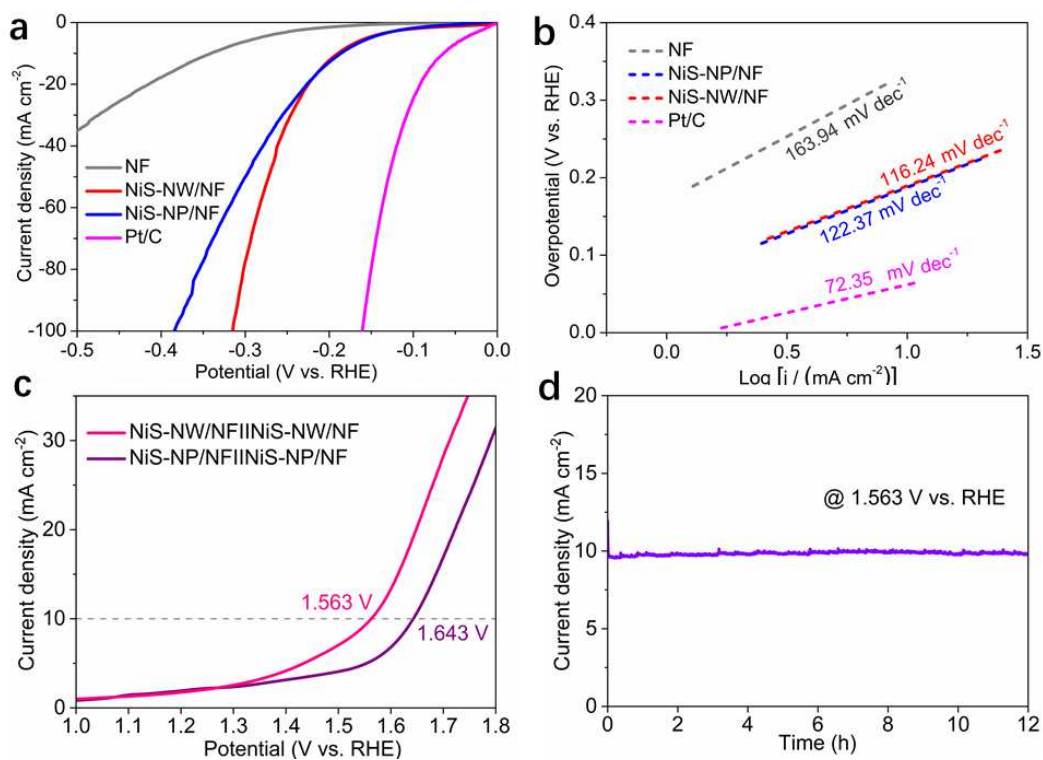
227

228 **Fig. 5** (a-c) Cyclic voltammograms of NiS-NW/NF, NiS-NW/NF, and nickel foam at different scan
 229 rates (from 40 to 120 mV s^{-1} with an increment of 20mV s^{-1}). (d) Scan rate dependence of the current
 230 densities of NiS-NW/NF, NiS-NW/NF, and nickel foam at 1.15 V vs. RHE, (e) Nyquist plots at the
 231 open circuit potential, (f) Amperometric i-t curve of NiS-NW/NF at an applied potential of 1.5 V versus
 232 RHE.

233 Moreover, the HER activity of NiS-NW/NF, NiS-NP/NF and NF was also measured in
 234 N_2 -saturated 1.0 M KOH. The overpotentials required to reach 20 mA cm^{-2} are determined to be
 235 224, 228, and 415 mV vs. RHE for NiS-NW/NF, NiS-NP/NF and NF, respectively (**Fig. 6a**). This
 236 comparison clearly shows that NiS-NW/NF exhibits a lower overpotential than NiS-NP/NF.
 237 However, the HER performances of NiS catalysts in this study are inferior to those of the 20 wt %
 238 Pt/C benchmark catalyst which only takes 92.6 mV to achieve a current density of 20 mA cm^{-2} .
 239 Although the 20 wt % Pt/C catalyst exhibits the smallest Tafel slope ($72.35 \text{ mV dec}^{-1}$), the Tafel
 240 slope of NiS-NW/NF ($116.24 \text{ mV dec}^{-1}$) is lower than that of NiS-NP/NF ($122.37 \text{ mV dec}^{-1}$) and

241 NF ($163.94 \text{ mV dec}^{-1}$) (**Fig. 6b**). These results suggest that NiS-NW/NF exhibits improved HER
242 activity compared to NiS-NP/NF, demonstrating the advantage of the dimensionally constructed
243 heterogeneous nanoworm structure with multi-level interfaces. Moreover, the excellent HER
244 performance of NiS-NW/NF is also attributed to abundant exposure of electroactive sites owing to
245 the high surface area. Apart from the favorable HER activity, NiS-NW/NF also shows good
246 durability in 1 M KOH. The results displayed in **Fig. S4** suggest the electrocatalytic activity of
247 hydrogen evolution decreases very little after 12 h electrocatalysis.

248 As the synthesized catalyst showcases good electrocatalytic activities toward both OER and HER
249 in the alkaline solution, a two-electrode single cell system was constructed using NiS-NW/NF as
250 both cathode and anode to investigate its overall water splitting competency. For comparison, the
251 performance of NiS-NP/NF was also tested. Impressively, the current density of 10 mA cm^{-2} is
252 achieved obtained at a low cell voltage of 1.563 V over the NiS-NW/NF||NiS-NW/NF, which is
253 smaller than that of 1.643 V over the NiS-NP/NF||NiS-NP/NF (**Fig. 6c**). At a constant potential of
254 1.563 V, NiS-NW/NF shows a negligible change of current density after continuous operation for
255 12 h (**Fig. 6d**), which indicates its great durability. As a catalyst for overall water splitting, the
256 NiS-NW/NF shows favorable catalytic activity and structural stability, directing an efficient and
257 large-scale synthetic strategy for binder-free catalysts in renewable energy conversion.



258

259 **Fig. 6** (a) LSV curves of the HER performance of NiS-NW/NF, NiS-NW/NF, nickel foam, and 20 wt %
 260 Pt/C, (b) corresponding Tafel plots, (c) LSV curve of water electrolysis using NiS-NW/NF or
 261 NiS-NW/NF as both HER and OER electrocatalysts in a two-electrode configuration, (d)
 262 Amperometric i-t curve of NiS-NW/NF for water splitting at an applied potential of 1.563 V.

263 4. Conclusions

264 In summary, we have synthesized a nanoworm-like nickel sulfide nanostructure via a one-step
 265 solvothermal method. With a smaller size, larger electrochemical surface area, and lower charge
 266 transfer resistance, the as-prepared nanoworm-like nickel sulfides (NiS-NW/NF) perform better
 267 than the nanoplate-like counterpart. The NiS-NW/NF only takes a low overpotential of 279 mV to
 268 obtain 100 mA cm^{-2} for OER, exceeding most of reported nickel sulfide-based catalysts. In
 269 addition, when used as a bifunctional catalyst for overall water splitting, the NiS-NW/NF achieves
 270 a current density of 10 mA cm^{-2} at only 1.563 V with good long-term durability. This study

271 provides a facile and effective strategy for the design and development of cost-effective catalysts
272 for water splitting.

273 **CRedit authorship contribution statement**

274 **Zhijie Chen:** Experiments, Conceptualization, Discussions, Writing. **Idris Ibrahim:** Material
275 synthesis, Discussions. **Derek Hao:** Writing, Data analysis, Discussions. **Xiaoqing Liu:** Data
276 analysis, Discussions. **Lan Wu:** Data analysis, Discussions. **Wei Wei:** Data analysis, Discussions.
277 **Dawei Su:** Data analysis, Discussions. **Bing-Jie Ni:** Discussions, Writing, Project acquisition.

278 **Declaration of Competing Interest**

279 The authors declare no competing financial interest.

280 **Acknowledgements**

281 This work is supported by the Australian Research Council (ARC) Future Fellowship
282 (FT160100195). Mr. Zhijie Chen acknowledges the China Scholarship Council (CSC) for the
283 scholarship support.

284 **References**

- 285 [1] H. Wan, X. Liu, H. Wang, R. Ma, T. Sasaki, Recent advances in developing high-performance
286 nanostructured electrocatalysts based on 3d transition metal elements, *Nanoscale Horiz.* 4 (2019)
287 789-808.
- 288 [2] Z. Chen, X. Duan, W. Wei, S. Wang, B.-J. Ni, Recent advances in transition metal-based
289 electrocatalysts for alkaline hydrogen evolution, *J. Mater. Chem. A* 7 (2019) 14971-15005.
- 290 [3] B. You, Y. Sun, Innovative strategies for electrocatalytic water splitting, *Acc. Chem. Res.* 51 (2018)
291 1571-1580.
- 292 [4] Q. Shi, S. Fu, C. Zhu, J. Song, D. Du, Y. Lin, Metal-organic frameworks-based catalysts for
293 electrochemical oxygen evolution, *Materials Horiz.* 6 (2019) 684-702.
- 294 [5] Z. Chen, X. Duan, W. Wei, S. Wang, Z. Zhang, B.-J. Ni, Boride-based electrocatalysts: Emerging
295 candidates for water splitting, *Nano Res.* 13 (2020) 293-314.

- 296 [6] Z. Chen, W. Wei, B.-J. Ni, Cost-effective catalysts for renewable hydrogen production via
297 electrochemical water splitting: Recent advances, *Curr. Opin. Green Sustain. Chem.* 27 (2021) 100398.
- 298 [7] L. Lv, Z. Yang, K. Chen, C. Wang, Y. Xiong, 2D layered double hydroxides for oxygen evolution
299 reaction: From fundamental design to application, *Adv. Energy Mater.* 9 (2019) 1803358.
- 300 [8] P. Yu, F. Wang, T.A. Shifa, X. Zhan, X. Lou, F. Xia, J. He, Earth abundant materials beyond
301 transition metal dichalcogenides: A focus on electrocatalyzing hydrogen evolution reaction, *Nano*
302 *Energy* 58 (2019) 244-276.
- 303 [9] J. Li, G. Zheng, One-dimensional earth-abundant nanomaterials for water-splitting electrocatalysts,
304 *Adv. Sci.* 4 (2017) 1600380.
- 305 [10] M.Q. Yang, J. Wang, H. Wu, G.W. Ho, Noble metal-free nanocatalysts with vacancies for
306 electrochemical water splitting, *Small* 14 (2018) e1703323.
- 307 [11] B. Zhu, R. Zou, Q. Xu, Metal-organic framework based catalysts for hydrogen evolution, *Adv.*
308 *Energy Mater.* 8 (2018) 1801193.
- 309 [12] S. Zhao, Y. Wang, J. Dong, C.-T. He, H. Yin, P. An, K. Zhao, X. Zhang, C. Gao, L. Zhang,
310 Ultrathin metal-organic framework nanosheets for electrocatalytic oxygen evolution, *Nat. Energy* 1
311 (2016) 1-10.
- 312 [13] X. Liu, L. Dai, Carbon-based metal-free catalysts, *Nat. Rev. Mater.* 1 (2016) 16064.
- 313 [14] C. Hu, L. Dai, Doping of carbon materials for metal-free electrocatalysis, *Adv. Mater.* 31 (2019)
314 e1804672.
- 315 [15] D. Liu, L. Dai, X. Lin, J.F. Chen, J. Zhang, X. Feng, K. Mullen, X. Zhu, S. Dai, Chemical
316 approaches to carbon-based metal-free catalysts, *Adv. Mater.* 31 (2019) e1804863.
- 317 [16] S. Zhao, D.W. Wang, R. Amal, L. Dai, Carbon-based metal-free catalysts for key reactions
318 involved in energy conversion and storage, *Adv. Mater.* 31 (2019) 1801526.
- 319 [17] S. Zhao, X. Lu, L. Wang, J. Gale, R. Amal, Carbon-based metal-free catalysts for electrocatalytic
320 reduction of nitrogen for synthesis of ammonia at ambient conditions, *Adv. Mater.* 31 (2019) 1805367.
- 321 [18] Y. Guo, T. Park, J.W. Yi, J. Henzie, J. Kim, Z. Wang, B. Jiang, Y. Bando, Y. Sugahara, J. Tang, Y.
322 Yamauchi, Nanoarchitectonics for transition metal sulfide based electrocatalysts for water splitting,
323 *Adv. Mater.* 31 (2019) 1807134.
- 324 [19] J. Hou, Y. Wu, B. Zhang, S. Cao, Z. Li, L. Sun, Rational design of nanoarray architectures for
325 electrocatalytic water splitting, *Adv. Funct. Mater.* 29 (2019) 1808367.
- 326 [20] J. Joo, T. Kim, J. Lee, S.I. Choi, K. Lee, Morphology-controlled metal sulfides and phosphides for
327 electrochemical water splitting, *Adv. Mater.* 31 (2019) e1806682.
- 328 [21] T. Sun, G. Zhang, D. Xu, X. Lian, H. Li, W. Chen, C. Su, Defect chemistry in 2D materials for
329 electrocatalysis, *Mater. Today Energy* 12 (2019) 215-238.
- 330 [22] Y. Zhang, L. Guo, L. Tao, Y. Lu, S. Wang, Defect-based single-atom electrocatalysts, *Small*
331 *Methods* 3 (2018) 1800406.
- 332 [23] T. Tang, W.-J. Jiang, S. Niu, L.-P. Yuan, J.-S. Hu, L.-J. Wan, Hetero-coupling of a carbonate
333 hydroxide and sulfide for efficient and robust water oxidation, *J. Mater. Chem. A* 7 (2019)
334 21959-21965.
- 335 [24] T.A. Shifa, F. Wang, Y. Liu, J. He, Heterostructures based on 2D materials: A versatile platform for
336 efficient catalysis, *Adv. Mater.* 31 (2018) e1804828.
- 337 [25] Z. Chen, X. Duan, W. Wei, S. Wang, B.-J. Ni, Iridium-based nanomaterials for electrochemical
338 water splitting, *Nano Energy* 78 (2020) 105270.
- 339 [26] X. Wu, X. Han, X. Ma, W. Zhang, Y. Deng, C. Zhong, W. Hu, Morphology-controllable synthesis

340 of Zn-Co-mixed sulfide nanostructures on carbon fiber paper toward efficient rechargeable zinc-air
341 batteries and water electrolysis, *ACS Appl. Mater. Interfaces* 9 (2017) 12574-12583.

342 [27] B. You, N. Jiang, Y.J. Sun, Morphology-activity correlation in hydrogen evolution catalyzed by
343 cobalt sulfides, *Inorg. Chem. Front.* 3 (2016) 279-285.

344 [28] Z. Chen, Y. Liu, W. Wei, B.-J. Ni, Recent advances in electrocatalysts for halogenated organic
345 pollutant degradation, *Environ. Sci.: Nano* 6 (2019) 2332-2366.

346 [29] Y. Guan, H. Xuan, H. Li, P. Han, Synthesis of 3D flower-like nickel-molybdenum-sulfur
347 microspheres as efficient and stable electrocatalyst for hydrogen and oxygen evolution reactions,
348 *Electrochim. Acta* 320 (2019) 134614.

349 [30] F. Wu, X. Guo, G. Hao, Y. Hu, W. Jiang, Synthesis of iron-nickel sulfide porous nanosheets via a
350 chemical etching/anion exchange method for efficient oxygen evolution reaction in alkaline media, *Adv.*
351 *Mater. Interfaces* 6 (2019) 1900788.

352 [31] B. Li, Z. Li, F. He, Q. Pang, P. Shen, One-pot preparation of Ni₃S₂@3-D graphene free-standing
353 electrode by simple Q-CVD method for efficient oxygen evolution reaction, *Int. J. Hydrogen Energy*
354 44 (2019) 30806-30819.

355 [32] W. He, G. Ren, Y. Li, D. Jia, S. Li, J. Cheng, C. Liu, Q. Hao, J. Zhang, H. Liu, Amorphous
356 nickel-iron hydroxide films on nickel sulfide nanoparticles for the oxygen evolution reaction, *Catal. Sci.*
357 *Technol.* 10 (2020) 1708-1713.

358 [33] J. Zhu, M. Sun, S. Liu, X. Liu, K. Hu, L. Wang, Study of active sites on Se-MnS/NiS
359 heterojunctions as highly efficient bifunctional electrocatalysts for overall water splitting, *J. Mater.*
360 *Chem. A* 7 (2019) 26975-26983.

361 [34] J. Lin, H. Wang, X. Zheng, Y. Du, C. Zhao, J. Qi, J. Cao, W. Fei, J. Feng, Controllable synthesis of
362 core-branch Ni₃S₂/Co₉S₈ directly on nickel foam as an efficient bifunctional electrocatalyst for overall
363 water splitting, *J. Power Sources* 401 (2018) 329-335.

364 [35] J.-F. Qin, M. Yang, S. Hou, B. Dong, T.-S. Chen, X. Ma, J.-Y. Xie, Y.-N. Zhou, J. Nan, Y.-M. Chai,
365 Copper and cobalt co-doped Ni₃S₂ grown on nickel foam for highly efficient oxygen evolution reaction,
366 *Appl. Surf. Sci.* 502 (2020) 144172.

367 [36] K.-L. Yan, X. Shang, Z. Li, B. Dong, J.-Q. Chi, Y.-R. Liu, W.-K. Gao, Y.-M. Chai, C.-G. Liu,
368 Facile synthesis of binary NiCoS nanorods supported on nickel foam as efficient electrocatalysts for
369 oxygen evolution reaction, *Int. J. Hydrogen Energy* 42 (2017) 17129-17135.

370 [37] Y. Zhao, B. Jin, A. Vasileff, Y. Jiao, S.-Z. Qiao, Interfacial nickel nitride/sulfide as a bifunctional
371 electrode for highly efficient overall water/seawater electrolysis, *J. Mater. Chem. A* 7 (2019)
372 8117-8121.

373 [38] S. Shit, S. Chhetri, W. Jang, N.C. Murmu, H. Koo, P. Samanta, T. Kuila, Cobalt sulfide/nickel
374 sulfide heterostructure directly grown on nickel foam: An efficient and durable electrocatalyst for
375 overall water splitting application, *ACS Appl. Mater. Interfaces* 10 (2018) 27712-27722.

376 [39] Y. Ding, H. Li, Y. Hou, Phosphorus-doped nickel sulfides/nickel foam as electrode materials for
377 electrocatalytic water splitting, *Int. J. Hydrogen Energy* 43 (2018) 19002-19009.

378 [40] Y. Zhou, S. Xi, X. Yang, H. Wu, In situ hydrothermal growth of metallic Co₉S₈-Ni₃S₂ nanoarrays
379 on nickel foam as bifunctional electrocatalysts for hydrogen and oxygen evolution reactions, *J. Solid*
380 *State Chem.* 270 (2019) 398-406.

381 [41] K. Wan, J. Luo, C. Zhou, T. Zhang, J. Arbiol, X. Lu, B.W. Mao, X. Zhang, J. Fransaer,
382 Hierarchical porous Ni₃S₄ with enriched high-valence Ni sites as a robust electrocatalyst for efficient
383 oxygen evolution reaction, *Adv. Funct. Mater.* 29 (2019) 1900315.

Highlights

1. The nanoworm-like nickel sulfides (NiS) were designed by a facile solvothermal process
2. The solvothermal precursors govern the nanostructure of NiS
3. The nanoworm-like NiS outperform the nanoplate-like counterpart for water splitting
4. The nanoworm-like NiS exhibit good activity and stability for overall water splitting